Supplementary Information for

A Remarkably Air-Stable Quinodimethane Radical Cation

Mei Harada,[‡a] Masaru Tanioka, [‡b] Atsuya Muranaka,*[c] Tetsuya Aoyama,[c] Shinichiro Kamino,[b] and Masanobu Uchiyama*[a,c,d]

[a]Graduate School of Pharmaceutical Sciences, The University of Tokyo, 7-3-1, Hongo, Bunkyo-ku, Tokyo 113-0033, Japan
[b]School of Pharmaceutical Sciences, Aichi Gakuin University, 1-100 Kusumoto-cho, Chikusa-ku, Nagoya 464-8650, Japan
[c]Cluster for Pioneering Research (CPR), Advanced Elements Chemistry Laboratory, RIKEN, 2-1 Hirosawa, Wako-shi, Saitama 351-0198, Japan
[d]Research Initiative for Supra-Materials (RISM), Shinshu University, 3-15-1 Tokida, Ueda, Nagano 386-8567, Japan

[‡]These authors contributed equally.

Table of Contents

1. Instrumentation and Materials

Instruments

Electronic absorption spectra were collected at room temperature on a JASCO V-670 spectrometer. CW-ESR spectra were measured at the X-band frequency (about 9100 MHz) with a JEOL JES-FA300 spectrometer using a quartz sample tube under ambient conditions. Instrumental acquisition parameters (center field = 325.00 mT, sweep width = 50 mT, modulation amplitude = 5.0 or 50 mT, modulation frequency = 100 kHz, power = 0.99800 mW, time constant = 0.03 s) were carefully chosen to avoid saturation effects and spectral line shape distortion. Mn^{2+} was used as an internal standard.

Materials

Reagents were purchased from FUJIFILM Wako, TCI, or Fukui Yamada Chemical, Japan. All solvents were used without further purification. Compound **1** was synthesized from commercially available 2-(4-dibutylamino-2-hydroxybenzoyl)benzoic acid and 1,4-dimethoxybenzene according to literature procedures.[1]

2. Computational Details

All calculations were performed at the Density Functional Theory (DFT) as implemented in Gaussian 16[2]. Geometry optimizations for $\mathbf{1_{Me}}^{\bullet+}$, $\mathbf{1_{Me}}$, and reference radicals were performed using the unrestricted B3LYP method with the 6-31G(d,p) basis set. Vibrational frequency calculations verified the nature of the stationary points. Spin density maps, Mulliken spin density values, and electrostatic potential (ESP) distributions were calculated at the same level as above. Excitation wavelengths and oscillator strengths were calculated by the TD-DFT approach. Energy differences between singlet and triplet states of two adjacent BTAQ radical cations in the X-ray structure ($(\mathbf{1_{Me}}^{\bullet+})_2$) were calculated using several functionals and basis sets.

3. Experimental Procedures

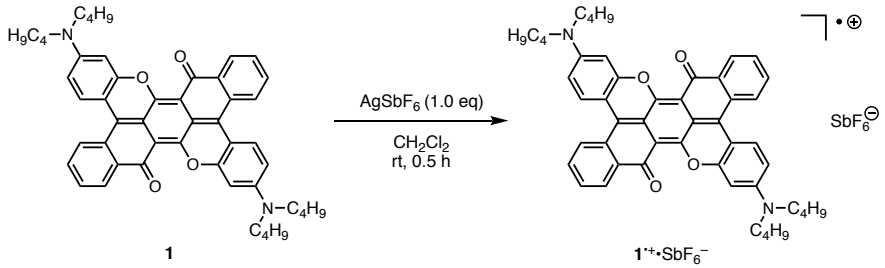

Synthesis of $\mathbf{1}^{\bullet+}\bullet\mathbf{SbF_6}^-$: To a solution of **1** (14.8 mg, 0.02 mmol) in CH_2Cl_2 (300 mL) was slowly added a solution of $AgSbF_6$ (6.9 mg, 0.02 mmol) in CH_2Cl_2/CH_3CN (4:0.1 v/v, 10 mL) at room temperature under Ar. After stirring for 0.5 h at this temperature, the reaction mixture was concentrated in vacuo and CH_2Cl_2 (10 mL) was added. The suspended solution was filtrated by Minisart Syringe Filter with the pore size of 0.2 μm. The filtrated solution was concentrated in vacuo to a powder which was dissolved in CH_2Cl_2 (2 mL). Toluene (10 mL) was added to the CH_2Cl_2 solution to give $\mathbf{1}^{\bullet+}\bullet SbF_6^-$ as a dark olive-green solid (18.2 mg, 93 %).

$\mathbf{1}^{\bullet+}\bullet SbF_6^-$: UV/vis/NIR ($CH_2Cl_2$): λ_{max} ($\varepsilon \times 10^{-4}$ (M^{-1} cm^{-1})) = 1303 (3.9), 1094 (1.2), 1007 (4.4), 927 (8.5) nm. HRMS (ESI, positive) *m/z* calcd. for $C_{50}H_{50}N_2O_4$ (M^+): 742.3771, found: 742.3798. FT-IR (ATR): $\tilde{\nu}_{max}$ = 2931, 2869, 1603, 1565, 1544, 1479, 1435, 1410, 1362, 1284, 1208, 1184, 1161, 1130, 1108, 921, 893, 822, 797, 781, 742, 723, 687, 650, 583, 554 cm^{-1}. ESR: g = 2.0035 (CH_2Cl_2 solution), 2.0007 (powder).

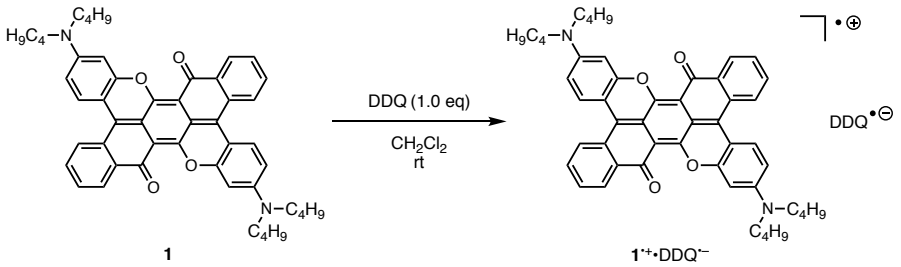

Preparation of $\mathbf{1}^{\bullet+}\bullet\mathbf{DDQ}^{\bullet-}$ solution: To a solution of **1** in CH_2Cl_2 was added a solution of equivalent amounts of DDQ in CH_2Cl_2 at room temperature. The resulting solution was used without further purification.

$\mathbf{1}^{\bullet+}\bullet DDQ^{\bullet-}$: UV/vis/NIR ($CH_2Cl_2$): λ_{max} ($\varepsilon \times 10^{-4}$ (M^{-1} cm^{-1})) = 1303 (3.5), 1095 (1.0), 1006 (4.0), 925 (7.6) nm. HRMS (ESI, positive) *m/z* calcd. for $C_{50}H_{50}N_2O_4$ (M^+): 742.3771, found: 742.3783. ESR: g = 2.0027 (CH_2Cl_2 solution).

4. Electrochemical Properties

Cyclic voltammetry measurements were carried out with a Hokuto Denko HZ-7000 voltammetric analyzer. The cell contained inlets for a glassy carbon disk working electrode of 3.0 mm diameter and a platinum-wire counter electrode. The reference electrode was $Ag/AgNO_3$ (0.1M in MeCN). The scan rate was 100 mV s^{-1} . Ferrocene (Fc) was used as an internal standard and potentials were referenced to Fc/Fc^+.

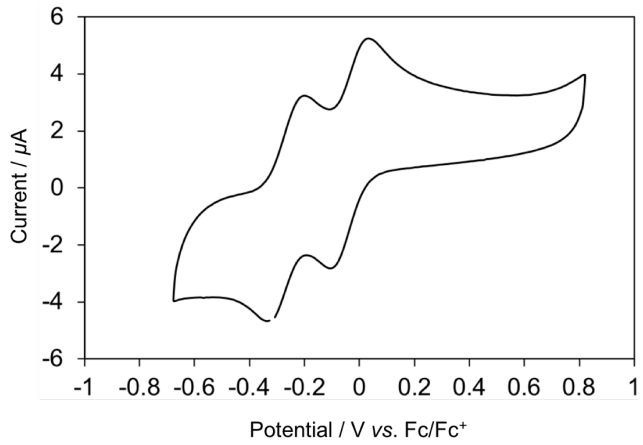

Figure S1. Cyclic voltammogram of **1** in 0.1 M n-Bu_4NClO_4/CH_2Cl_2 solution under air. The oxidation potentials ($E_{ox}^{1/2}$) determined from the midpoints of these oxidation peaks are –0.25 and –0.02 V.

5. ESR Spectra

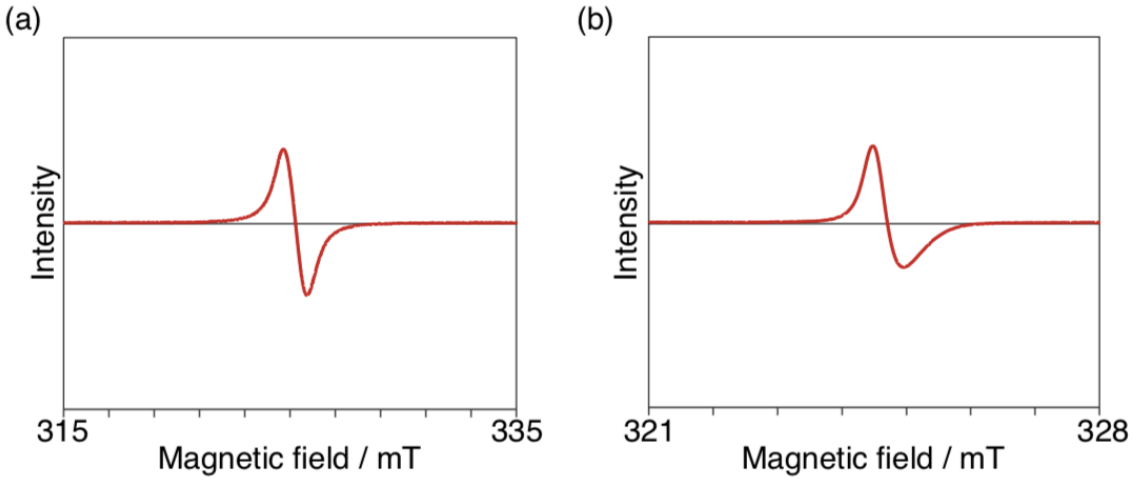

Figure S2. (a) Solid-state ESR spectrum of $\mathbf{1}^{\bullet+}\bullet SbF_6^-$ (g = 2.0007, ΔH_{msl} = 1.07 mT) under ambient conditions. Modulation amplitude 5.0 mT; modulation frequency 100.00 kHz. (b) ESR spectrum of a 1:1 mixture of **1** (0.5 mM) and DDQ (g = 2.0027, ΔH_{msl} = 0.48 mT) in CH_2Cl_2 under ambient conditions. Modulation amplitude 50 mT; modulation frequency 100.00 kHz. ΔH_{msl} indicates the maximum slope line width.

6. Optical Properties

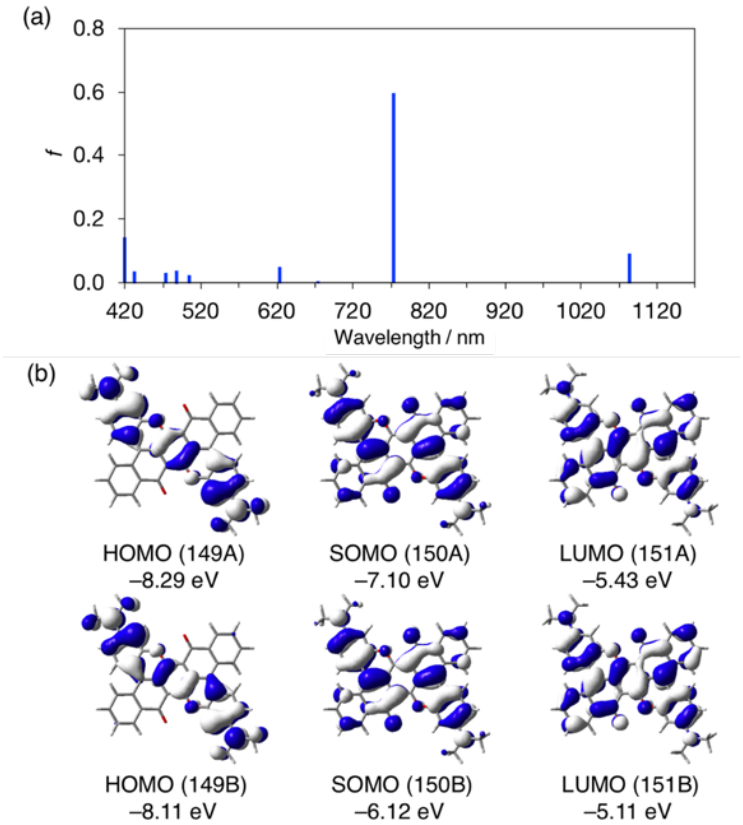

Figure S3. (a) Calculated absorption spectrum of $\mathbf{1_{Me}}^{\bullet+}$. (b) Frontier molecular orbitals. Calculations were performed at the UB3LYP/6-31G(d,p) level.

Table S1. Calculated excitation wavelength (nm), oscillator strength (*f*), electric transition dipole moment (au), and major contribution (%) for $\mathbf{1_{Me}}^{\bullet+}$ (UB3LYP/6-31G(d,p)).

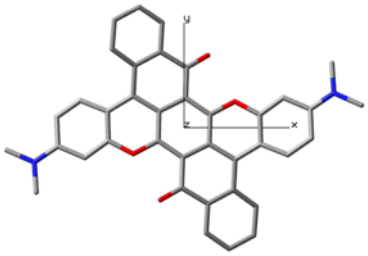

	λ / nm	f	μ (x, y, z) / au	Contribution (%)
1	1086	0.09	1.41, –1.13, 0.00	150A → 151A (76.9), 149B → 150B (20.4)
2	776	0.59	–3.87, 0.09, –0.12	149B → 150B (73.9), 150A → 151A (19.2)

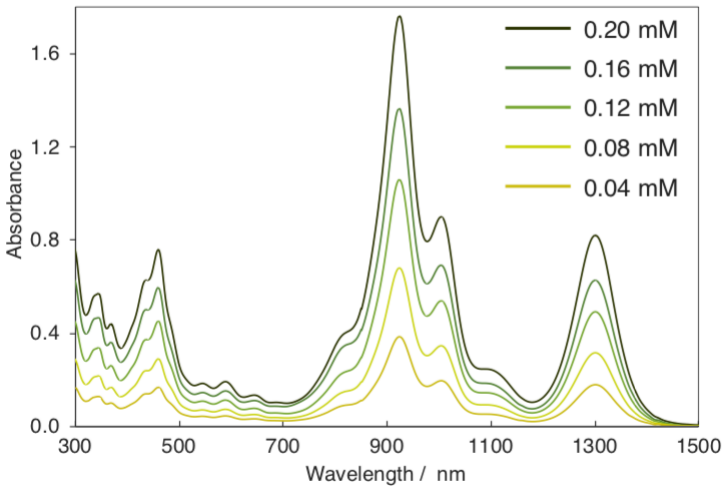

Figure S4. Concentration dependence of the electronic absorption spectra of $\mathbf{1}^{\bullet+}$•$DDQ^{\bullet-}$ in CH_2Cl_2 at room temperature. A 1 mm quartz cell was used for the measurements.

7. Stability Experiments

A stability test of $\mathbf{1}^{\bullet+}\bullet SbF_6^-$ against silica-gel column chromatography was carried out using a silica-gel column (Wako-gel C-200E, ϕ 6 × 35 mm, CH_2Cl_2/CH_3OH = 100 : 6). Storage stability experiments were performed as follows. A 25 ml CH_2Cl_2 solution of each sample was prepared and stored in a capped volumetric flask on the bench. The concentration was adjusted so that the maximum absorption wavelength was ca. 1.0. The maximum absorption wavelengths used for $\mathbf{1}^{\bullet+}\bullet SbF_6^-$, $\mathbf{1}^{\bullet+}\bullet DDQ^{\bullet-}$, $\mathbf{2}^{\bullet+}\bullet SbCl_6^-$, galvinoxyl radical were 1303, 1303, 728, and 433 nm, respectively. As the volume of CH_2Cl_2 solution slightly decreased during the storage period, a small amount of CH_2Cl_2 was added to keep constant concentration. No significant spectral changes were observed for the isolated radical cation salt ($\mathbf{1}^{\bullet+}\bullet SbF_6^-$, Fig. 3a) and a 1:1 mixture of **1** and $AgSbF_6$ (Fig. S6).

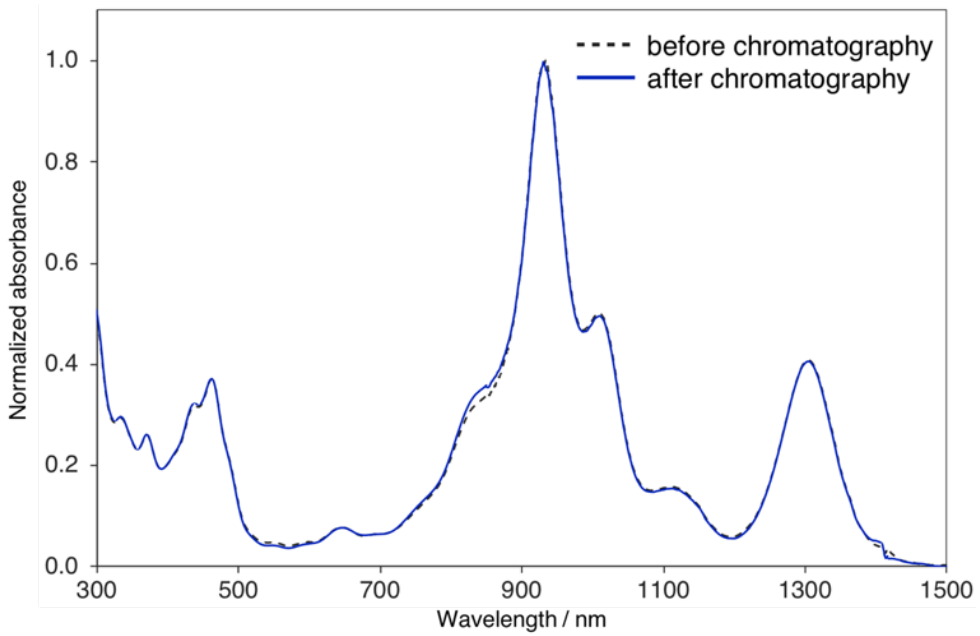

Figure S5. Electronic absorption spectra of $\mathbf{1}^{\bullet+}\bullet SbF_6^-$ in CH_2Cl_2/CH_3OH = 100 : 6 before (blue solid line) and after (black broken line) silica-gel column chromatography.

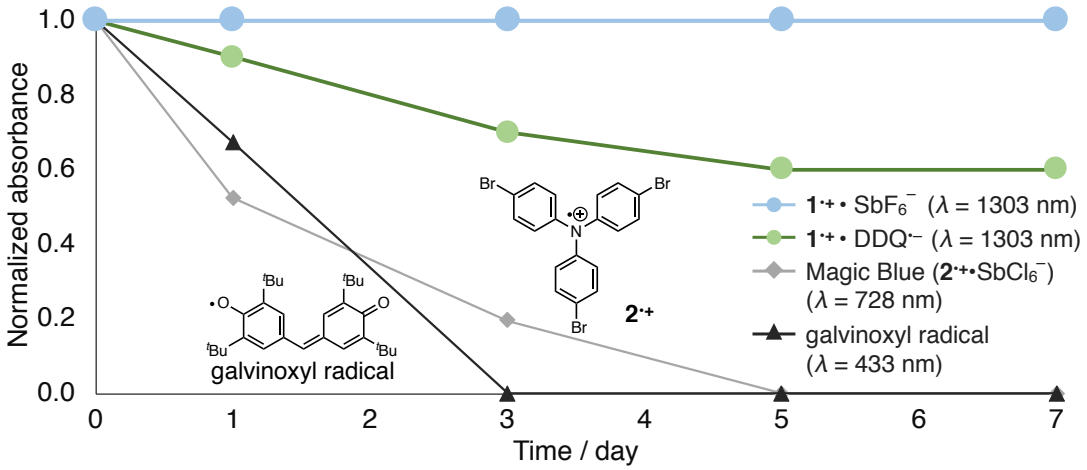

Figure S6. Effects of storage period on the absorbance of CH_2Cl_2 solutions of $\mathbf{1}^{\bullet+}$•SbF_6^-, $\mathbf{1}^{\bullet+}$•$DDQ^{\bullet-}$, Magic Blue ($\mathbf{2}^{\bullet+}$•$SbCl_6^-$), and galvinoxyl radical. Each solution was stored under room light (fluorescent light) at room temperature. The normalized absorbance was based on the absorbance at the time of solution preparation. The solution of $\mathbf{1}^{\bullet+}$•SbF_6^- was prepared by mixing equimolar amounts of **1** and $AgSbF_6$.

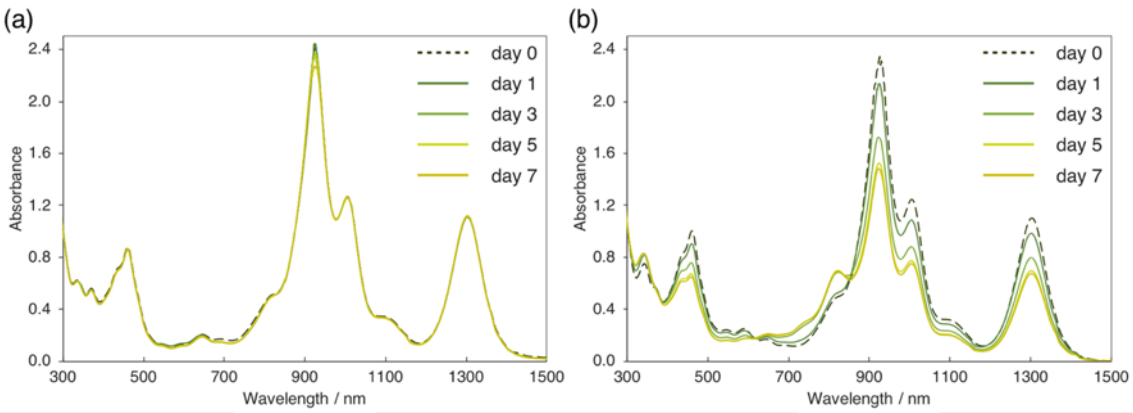

Figure S7. Electronic absorption spectra of (a) $\mathbf{1}^{\bullet+}$•SbF_6^- and (b) $\mathbf{1}^{\bullet+}$•$DDQ^{\bullet-}$ in CH_2Cl_2 under room light (fluorescent light) at room temperature.

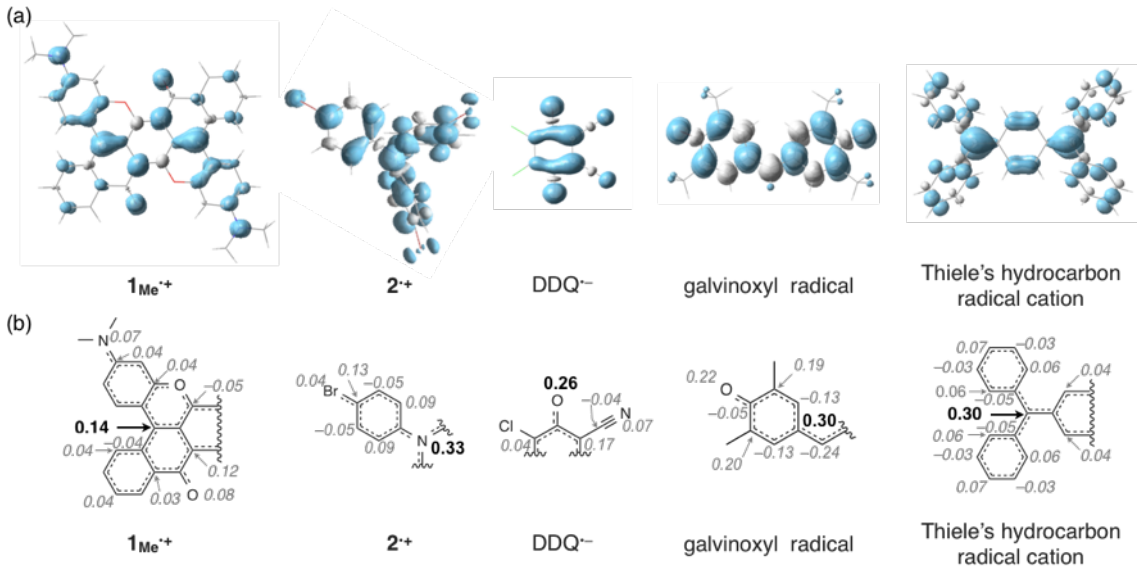

Figure S8. (a) Spin density maps (isovalue = 0.002, light blue: positive spin, white: negative spin) of $\mathbf{1}_{Me}^{\bullet+}$, $\mathbf{2}^{\bullet+}$, DDQ$^{\bullet-}$, galvinoxyl radical, and Thiele's hydrocarbon radical cation. (b) Selected Mulliken spin density values. The absolute values more than 0.03 were shown. Calculations were performed at the UB3LYP/6-31G(d,p) level. *tert*-Butyl groups of galvinoxyl radical were replaced with methyl groups.

8. Single X-ray Structure Analysis

Single crystals of $\mathbf{1}^{\bullet+}$•$DDQ^{\bullet-}$ were obtained by slow diffusion of diethyl ether into a CH_2Cl_2 solution of **1** with two equivalents of DDQ at 10°C. Single crystals of **1** were obtained by slow diffusion of CH_3OH into a CH_2Cl_2 solution at 10°C. The single crystals were mounted on a glass capillary and set on a Rigaku XtaLAB Synergy-S diffractometer. The diffraction data were collected using Cu Kα radiation, which was monochromated by a multi-layered confocal mirror. The structure was solved by a direct method and refined on F^2 by a least squares method by the program SHELXL[3,4]. All non-hydrogen atoms were refined anisotropically. All the hydrogen atoms were put on calculated geometrically, and were refined by applying riding models. Structural drawings and geometrical calculations were performed with ORTEP[5] and PLATON[6], respectively. Crystal data, structure refinement and included solvents are summarized in Table S2. Crystallographic data have been deposited with the Cambridge Crystallographic Data Centre: Deposition code CCDC 1990118 ($\mathbf{1}^{\bullet+}$•$DDQ^{\bullet-}$); 1990124 (**1**).

Table S2. Crystal data and structure refinement for $\mathbf{1}^{\bullet+}$•$DDQ^{\bullet-}$ and **1**.

	$\mathbf{1}^{\bullet+}$•$DDQ^{\bullet-}$	**1**
Chemical formula	$C_{59}H_{54}Cl_4N_4O_7$	$C_{52}H_{58}N_2O_6$
Recrystallization solvent	CH_2Cl_2 / Et_2O	CH_2Cl_2 / MeOH
Included solvent	CH_2Cl_2, H_2O	MeOH
Crystal system	Triclinic	Triclinic
Space group [no.]	*P*-1	*P*-1
Crystal color, habit	Dark brown, fibrous	Clear light red, prism
Crystal size, mm	0.26 × 0.07 × 0.06	0.40 × 0.09 × 0.09
a, Å	7.3092(2)	7.7428(4)
b, Å	18.6978(6)	9.3733(5)
c, Å	20.9767(5)	15.0192(11)
α, °	114.686(3)	78.867(5)
β, °	94.742(2)	76.566(5)
γ, °	99.943(3)	81.762(4)
Volume, Å^3	2527.02(14)	1034.70(11)
Z	2	1
D_{calcd}, g/cm^3	1.410	1.295
T, K	93	93
Radiation	Cu Kα	Cu Kα
M, mm^{-1}	2.621	0.665
$2\theta_{max}$ °	74.5	75.7
F(000)	1120	432
Reflns collected	9876	3782
Unique reflns	7390	3194
No. of parameters	801	320
R1 (*I* > 2.00σ(i))	0.0758	0.0741
R (all reflection)	0.1040	0.0856
GOF	1.097	1.078

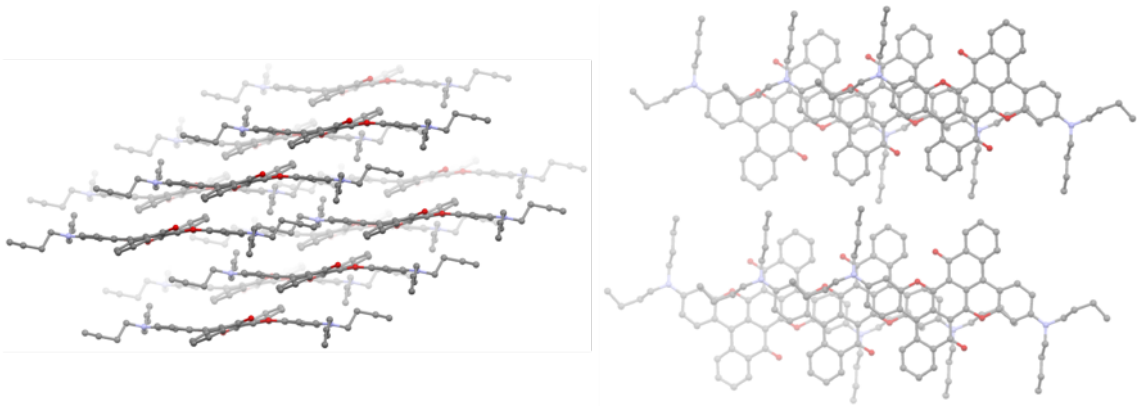

Figure S9. Crystal packing structures of **1**. Solvent molecules are omitted for clarity.

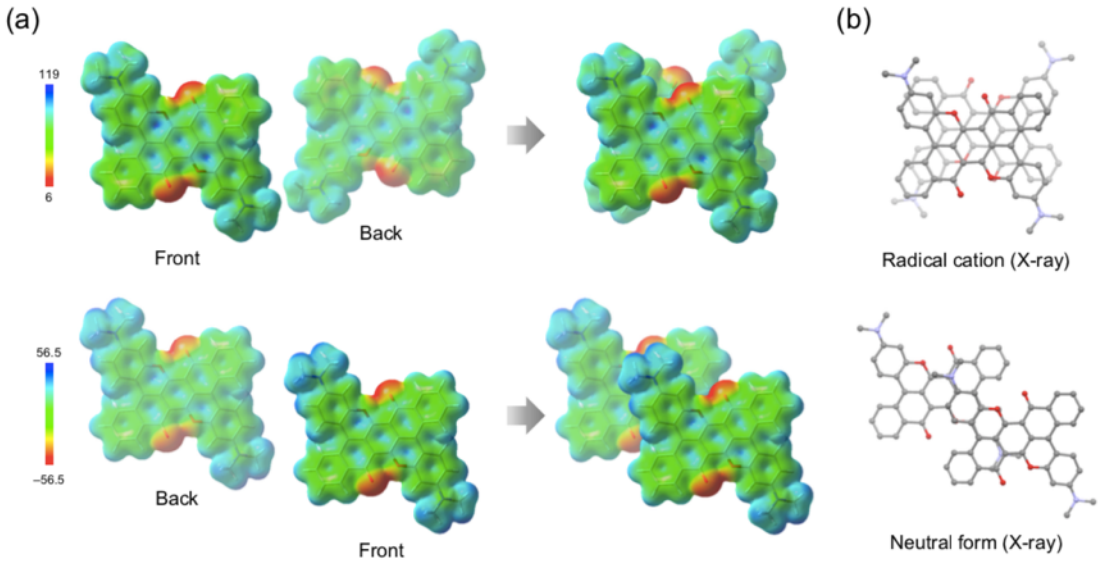

Figure S10. (a) Schematic illustration of overlap of electrostatic potential (ESP) distributions in two adjacent BTAQ molecules. ESP distributions (isovalue = 0.008) of $\mathbf{1_{Me}}^{\bullet+}$ (top) and $\mathbf{1_{Me}}$ (bottom) were calculated at the (U)B3LYP/6-31G(d,p) level. (b) π-Stacking of two adjacent BTAQs in the X-ray structures of $\mathbf{1}^{\bullet+}$•$DDQ^{\bullet-}$ (top) and **1** (bottom).

Table S3. Energy differences between singlet and triplet states of two adjacent BTAQ radical cations in the X-ray structure (($\mathbf{1_{Me}}^{\bullet+}$)$_2$).

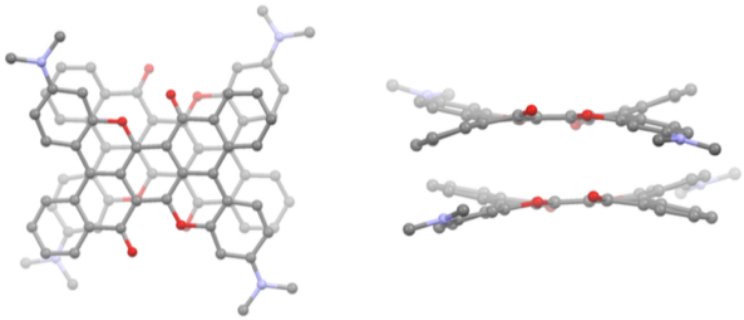

Computational level	E_S / hartree[a]	E_T / hartree[b]	ΔE / kcal/mol[c]
UB3LYP-D3/6-31G(d,p)	–3748.077689	–3748.082577	–3.1
UB3LYP-D3/6-311G(d,p)	–3748.851801	–3748.856650	–3.0
UB3LYP/6-31G(d,p)	–3747.835361	–3747.840249	–3.1
UωB97XD/6-31+G(d,p)	–3746.733103	–3746.751487	–11.5
UM06-2X/6-31G(d,p)	–3746.373352	–3746.385884	–7.9

[a]E_S: singlet state energy. [b]E_T: triplet state energy. [c]$\Delta E = E_T - E_S$.

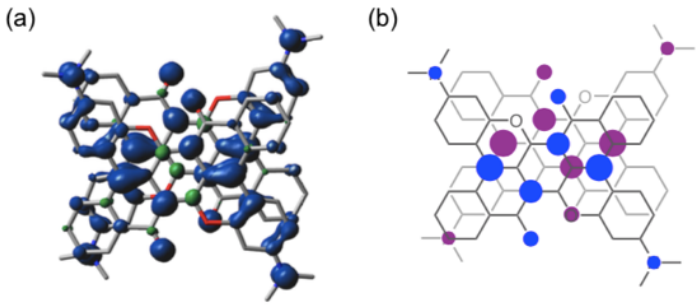

Figure S11. (a) Spin density map (triplet, isovalue = 0.002, dark blue: positive spin, green: negative spin) of ($\mathbf{1_{Me}}^{\bullet+}$)$_2$ calculated at the UB3LYP-D3/6-31G(d,p) level. (b) Schematic illustration of overlap of the spin densities.

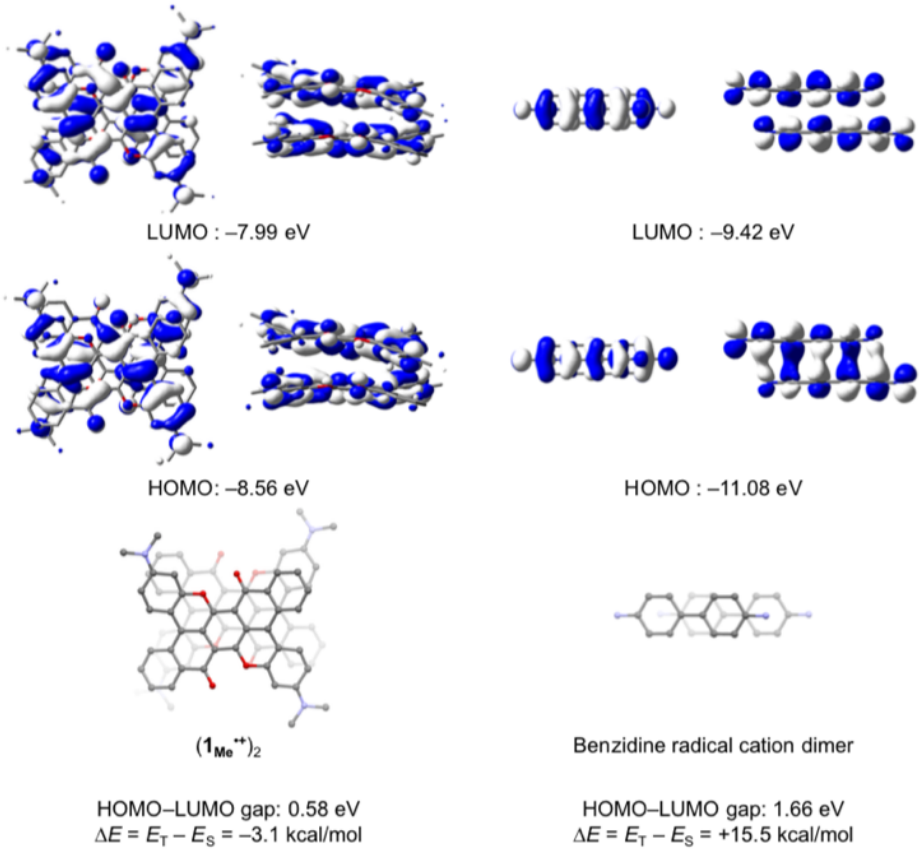

Figure S12. Frontier molecular orbitals (alpha orbitals, singlet, isovalue = 0.02) of $(\mathbf{1}_{Me}^{\bullet+})_2$ and a typical π-dimer (benzidine radical cation dimer[7]), showing no effective interactions between the SOMOs of $\mathbf{1}_{Me}^{\bullet+}$. Calculations were performed for the X-ray geometries at the UB3LYP-D3/6-31G(d,p) level. ΔE indicates the energy difference between singlet and triplet states ($\Delta E = E_T - E_S$).

8. Electric Properties

Fabrication and characterization of transistors with the neutral form (1)

Silicon substrates with a thermally grown 300 nm thick SiO_2 layer were ultrasonicated sequentially in pure water, 2-propanol, acetone, and then chloroform for 10 min each. They were then kept in an ozone atmosphere for 3 min, using a UV-ozone cleaner (PL16-110D, SEN Lights Corp.). Films of **1** with a thickness of 5 nm were spin-coated from about 1 mg mL^{-1} dichloromethane solution at 300 rpm on top of the substrates and then dried in vacuum at room temperature. Gold source/drain interdigitated electrodes were thermally evaporated through a shadow mask to complete bottom-gate top-contact transistors. The channel width and length were 15 mm and 50 μm, respectively. A couple of picoammeter/voltage source units (Keithley, model 6487) were used to measure the electrical properties of the devices.

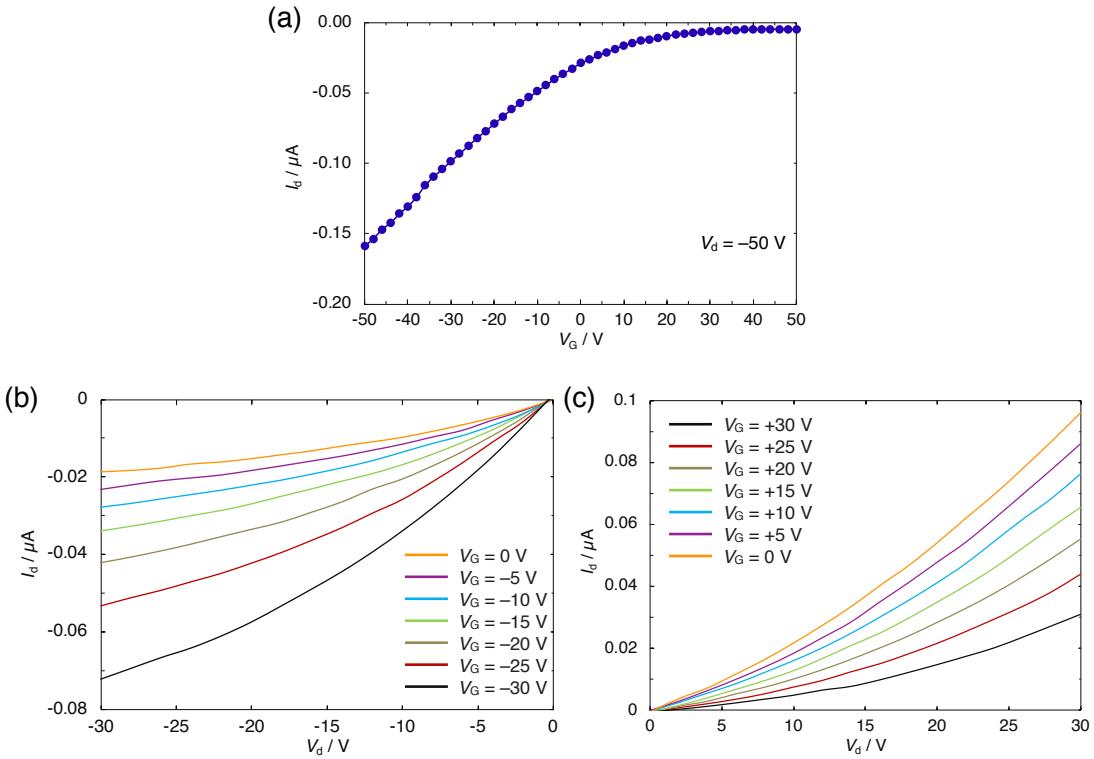

Figure S13. (a) Transfer and (b,c) output characteristics of a transistor with **1**.

Device fabrication and measurement for *I-V* characteristics in $\mathbf{1}^{\bullet+}$•$\mathbf{DDQ}^{\bullet-}$

The device fabrication processes were the same as those for the transistors with the neutral form (**1**). The films of $\mathbf{1}^{\bullet+}$•$DDQ^{\bullet-}$ with a thickness of 12 nm were obtained by spin coating from a 1 mg mL^{-1} dichloromethane solution. The *I-V* characteristics were measured with a picoammeter/voltage source unit (Keithley, model 6487) probing the gold electrodes to determine the resistance of the films. The conductivity was determined by the measured resistance and the geometry of the conduction path, using the equation of $\sigma = L/(RWd)$, where σ is the conductivity, R is the resistance, L is the channel length, W is the channel width, and d is the film thickness.[8,9]

10. Cartesian Coordinates (in Å) and Energies

$\mathbf{1_{Me}}^{\bullet+}$

E(UB3LYP) = -1873.97413844 A.U.

O	-2.40711600	-1.25388100	-0.35931400
O	-1.12449300	-3.45772100	-0.88071500
N	-7.10396800	-1.65260300	0.08742500
C	2.41615300	-1.52194400	0.02112200
C	2.34231100	-2.97426900	0.13907400
C	1.19260300	-0.78228600	-0.01346300
C	-3.59033100	-0.62216600	-0.13929000
C	1.12507100	-3.63041100	-0.17237400
C	-0.06986000	-1.41728900	-0.21641000
C	-1.22732200	-0.62743800	-0.18047000
C	-0.11824700	-2.87668900	-0.48264000
C	3.30769100	-5.14678500	0.68346800
H	4.14158200	-5.72830500	1.06370800
C	3.63358700	-0.78386600	-0.06712300
C	6.03996500	-0.50913300	-0.43406400
H	6.97949500	-0.95483400	-0.73242200
C	-5.98112400	-0.88587400	0.10835500
C	-4.70608100	-1.43636200	-0.15250100
H	-4.55242600	-2.48875300	-0.34584900
C	4.91892200	-1.29882400	-0.40744500
H	5.01041300	-2.33336300	-0.70934500
C	-7.00737900	-3.08305400	-0.19607300
H	-6.54407000	-3.26014400	-1.17281400
H	-8.00751500	-3.51279600	-0.21158700
C	2.12957700	-5.78785500	0.28235300
H	2.05484400	-6.86972100	0.32429200
C	1.04152000	-5.02693500	-0.12666200
H	0.09669900	-5.48503100	-0.39693600
C	3.41373200	-3.76387200	0.61492300
H	4.31404200	-3.28948700	0.98226500
C	-8.41042700	-1.07577100	0.40085700
H	-9.17577100	-1.83761900	0.26238500
H	-8.64406500	-0.23824700	-0.26467200
O	2.40715600	1.25384200	0.35939900
O	1.12457400	3.45768900	0.88074100
N	7.10394000	1.65269800	-0.08781000
C	-2.41610300	1.52189700	-0.02100500
C	-2.34228600	2.97421800	-0.13886300
C	-1.19255700	0.78223700	0.01359400
C	3.59036300	0.62214300	0.13929500
C	-1.12504300	3.63036600	0.17255600
C	0.06990300	1.41724200	0.21654700
C	1.22736300	0.62739100	0.18059300
C	0.11829000	2.87664400	0.48277900
C	-3.30779800	5.14673200	-0.68298800
H	-4.14175500	5.72825500	-1.06307800
C	-3.63355000	0.78384500	0.06710300
C	-6.03998200	0.50921800	0.43369900
H	-6.97954400	0.95496800	0.73188200
C	5.98111600	0.88593500	-0.10862500
C	4.70608900	1.43637300	0.15240100
H	4.55242300	2.48875600	0.34578700
C	-4.91891400	1.29887600	0.40718500
H	-5.01041100	2.33346000	0.70895000
C	7.00734500	3.08313300	0.19576200
H	6.54415900	3.26016700	1.17257100
H	8.00747100	3.51290400	0.21116400
C	-2.12964600	5.78780600	-0.28198200
H	-2.05494900	6.86967600	-0.32385800
C	-1.04153000	5.02689300	0.12689900
H	-0.09670400	5.48500200	0.39713300
C	-3.41379900	3.76381400	-0.61450600
H	-4.31416600	3.28941300	-0.98170600
C	8.41037400	1.07592000	-0.40144800
H	9.17571200	1.83778700	-0.26304800
H	8.64413100	0.23837500	0.26401200
H	6.41999600	3.60553400	-0.56876800
H	8.46160800	0.72625100	-1.43946500
H	-6.42014500	-3.60543900	0.56855600
H	-8.46179400	-0.72605400	1.43885100

11. References

1) Y. Okamoto, M. Tanioka, A. Muranaka, K. Miyamoto, T. Aoyama, X. Ouyang, S. Kamino, D. Sawada and M. Uchiyama, *J. Am. Chem. Soc.*, 2018, **140**, 17857.
2) Gaussian 16, Revision A.03, M. J. Frisch, G. W. Trucks, H. B. Schlegel, G. E. Scuseria, M. A. Robb, J. R. Cheeseman, G. Scalmani, V. Barone, G. A. Petersson, H. Nakatsuji, X. Li, M. Caricato, A. V. Marenich, J. Bloino, B. G. Janesko, R. Gomperts, B. Mennucci, H. P. Hratchian, J. V. Ortiz, A. F. Izmaylov, J. L. Sonnenberg, D. Williams-Young, F. Ding, F. Lipparini, F. Egidi, J. Goings, B. Peng, A. Petrone, T. Henderson, D. Ranasinghe, V. G. Zakrzewski, J. Gao, N. Rega, G. Zheng, W. Liang, M. Hada, M. Ehara, K. Toyota, R. Fukuda, J. Hasegawa, M. Ishida, T. Nakajima, Y. Honda, O. Kitao, H. Nakai, T. Vreven, K. Throssell, J. A. Jr. Montgomery, J. E. Peralta, F. Ogliaro, M. J. Bearpark, J. J. Heyd, E. N. Brothers, K. N. Kudin, V. N. Staroverov, T. A. Keith, R. Kobayashi, J. Normand, K. Raghavachari, A. P. Rendell, J. C. Burant, S. S. Iyengar, J. Tomasi, M. Cossi, J. M. Millam, M. Klene, C. Adamo, R. Cammi, J. W. Ochterski, R. L. Martin, K. Morokuma, O. Farkas, J. B. Foresman and D. J. Fox, Gaussian, Inc., Wallingford CT, 2016.
3) G. M. Sheldrick, *Acta Crystallogr. Sect. C*, 2015, **C71**, 3.
4) G. M. Sheldrick, *Acta Crystallogr. Sect. A*, 2008, **A64**, 112.
5) L. J. Farrugia, *J. Appl. Crystallogr*., 1997, **30**, 565.
6) A. L. Spek, *J. Appl. Crystallogr.*, 2003, **36**, 7.
7) X. Chen, B. Ma, X. Wang, S. Yao, L. Ni, Z. Zhou, Y. Li, W. Huang, J. Ma, J. Zuo and X. Wang, *Chem. Eur. J.*, 2012, **18**, 11828.
8) P. Coppo, R. Schroeder, M. Grell and M. L. Turner, *Synth. Metals*, 2004, **143**, 203.
9) H. Duan, C. C. Yuan, N. Becerra, L. J. Small, A. Chang, J. M. Gregoire and R. B. van Dover, *ACS Comb. Sci.*, 2013, **15**, 273.